catalysts

MDPI

Article

Effect of the Active Metal on the NO_x Formation during Catalytic Combustion of Ammonia SOFC Off-Gas

Tobias Weissenberger *, Ralf Zapf, Helmut Pennemann and Gunther Kolb

Fraunhofer Institute for Microengineering and Microsystems IMM, Carl-Zeiss-Straße 18-20, 55129 Mainz, Germany

* Correspondence: tobias.weissenberger@imm.fraunhofer.de

Abstract: Catalytic combustion of hydrogen and ammonia containing off-gas surrogate from an ammonia solid oxide fuel cell (SOFC) was studied with a focus on nitrogen oxides (NO_x) mitigation. Noble and transition metals (Pt, Pd, Ir, Ru, Rh, Cu, Fe, Ni) supported on Al_2O_3 were tested in the range of 100 to 800 °C. The tested catalysts were able to completely convert hydrogen and ammonia present in the off-gas. The selectivity to NO_x increased with reaction temperature and stagnated at temperatures of 600 °C and higher. At low temperatures, the formation of N_2O was evident, which declined with increasing temperature until no N_2O was observed at temperatures exceeding 400 °C. Over nickel and iridium-based catalysts, the NO_x formation was reduced drastically, especially at 300 to 400 °C. To the best knowledge of the authors, the current paper is the first study about catalytic combustion of hydrogen-ammonia mixtures as a surrogate of an ammonia-fed SOFC off-gas.

Keywords: ammonia; selective catalytic oxidation; SCO; SOFC; solid oxide fuel cell; catalytic combustion; nitrogen oxides; microreactor

Citation: Weissenberger, T.; Zapf, R.; Pennemann, H.; Kolb, G. Effect of the Active Metal on the NO_x Formation during Catalytic Combustion of Ammonia SOFC Off-Gas. *Catalysts* **2022**, *12*, 1186. https://doi.org/10.3390/catal12101186

Academic Editor: Antonio Vita

Received: 30 August 2022
Accepted: 28 September 2022
Published: 7 October 2022

1. Introduction

The maritime transport of goods emits less CO_2 per ton of cargo and km compared to other modes of transport. However, since a large part of international trade is transported by ship, the CO_2 emissions caused by international maritime shipping are immense [1,2].

Thus, global shipping is responsible for about 3% of the global greenhouse gas emissions (GHG) [3]. To reduce the negative impact of the shipping industry, the International Maritime Organization has set the goal to reduce the global CO_2 emission of the maritime shipping sector by at least 50%, compared to the emissions in the year 2008 [4].

To achieve this massive reduction in GHG emissions associated with shipping, environmentally friendly fuels and power systems must be introduced.

Fuel cells convert chemical energy directly into electrical energy, which results in a much higher efficiency compared to internal combustion engines [5]. The most common energy carrier used in fuels cells is hydrogen, which allows the operation of the fuel cell without emissions of CO_2 or other pollutants. Therefore, fuel cells are a very promising technology for the green energy generation, especially in transport applications such as maritime shipping.

However, when used as transportation fuel, the low energy density and high flammability of hydrogen represents major challenges. To increase the energy density, hydrogen must be stored at very high pressures, often exceeding 300 bar, or in liquid state at cryogenic temperatures [6]. High pressure and cryogenic hydrogen storage come with much higher energy demand for compression and cooling, respectively. Further, the necessary high-pressure tanks and compressors as well as the cooling system increase the investment costs drastically.

An attractive alternative for the direct hydrogen storage is the use of hydrogen carriers, which can be handled and stored under atmospheric or near atmospheric pressures and ambient temperatures [7].

One promising hydrogen carrier is ammonia due to advantages in terms of energy density, flammability and its possible direct use in solid oxide fuel cells (SOFC) [8]. Ammonia can be liquefied at 20 °C at a moderate pressure of 8.6 bar [9,10]. The lower storage pressure makes the tanks for liquefied ammonia much cheaper than the high-pressure tanks necessary for storage of compressed hydrogen or the cryogenic equipment necessary for storage of liquefied hydrogen. Therefore, the cost of ammonia storage per kWh would be much cheaper compared to storage of pure hydrogen [11].

Another advantage of ammonia as hydrogen carrier is the possibility of its direct conversion in SOFCs without the requirement for cracking reactor. The ammonia is decomposed into hydrogen and nitrogen directly in the SOFC due to its high operation temperature and the nickel catalyst present. Therefore, ammonia-fed SOFCs have attracted much interest for energy generation [12–14].

Recently, the European Union awarded funding for the ShipFC project to convert the world's first offshore vessel to run on ammonia-powered fuel cells under its Fuel Cells and Hydrogen Joint Undertaking (FCH JU) of the Research and Innovation program Horizon 2020. The ShipFC project consists of a consortium of 14 European companies and institutions and aims to install a 2 MW ammonia solid oxide fuel cell system on a shipping vessel to demonstrate that zero emission large-scale shipping is feasible. Thus, current SOFC systems will be scaled up to 2 MW and installed on the vessel Viking Energy in 2023 and operated for 3000 h during a one-year period. In addition to shipping, ammonia-powered SOFCs are an emerging technology for other mobile and stationary applications and can help to store and distribute energy form renewable sources such as wind and solar energy [15].

SOFCs and all other fuel cells cannot convert the fuel completely. Therefore, the fuel cell anode off-gas contains small quantities of unreacted hydrogen, even when a recycle of the off-gas back into the fuel cell is installed. The remaining hydrogen in the off-gas must be removed before releasing it to the atmosphere, which is commonly performed by combustion in a catalytic afterburner which also generates heat [14]. The heat generated in the afterburner can be used to preheat the ammonia and air feed before the fuel cell and excess heat can be used for heating on the vessel itself, increasing the overall efficiency of the SOFC system. In addition to hydrogen, the off-gas also contains traces of unconverted ammonia which must be removed in the catalytic afterburner too. Combustion of the ammonia traces would lead to relatively low NO_x emissions, due to the low NH_3 concentration in the feed. Nevertheless, selective catalytic oxidation of the ammonia to water and nitrogen is much preferred. Hence, the catalytic afterburner must be able to completely remove hydrogen and ammonia via combustion, while minimizing the formation of NO_x species.

In the literature, different studies about the catalytic ammonia combustion can be found. The studies could demonstrate that different catalysts are effective for the selective catalytic oxidation (SCO) of ammonia into nitrogen and water rather than NO_x, with nitrogen selectivities of up to 99% [16]. The tested catalysts include supported noble metals such as platinum [17], palladium [18], iridium [19], ruthenium [20], rhodium [21], silver [22] and gold [23]. Platinum-based catalysts showed relative low nitrogen selectivities while rhodium, palladium and silver reached selectivities of up to 97%. Another class of highly active NH_3 SCO catalysts are transition metals, e.g., iron [24], copper [25,26], cobalt [27], nickel [28], manganese [29], molybdenum [30] and vanadium [31]. Copper-based catalysts showed by far the highest nitrogen selectivities of the transition metal-based catalysts, converting up to 99% of the ammonia into nitrogen [32]. Bimetallic catalysts based on Pt/Rh and Pt/Pd have also been studied and have proven to be effective NH_3 SCO catalysts [33,34]. Further, catalysts based on mixed oxides such as Cu-Ce-Zn, Fe-Mg-Al or Cu-Mg-Al have also been studied for NH_3 SCO [35–37]. Common support materials for NH_3 SCO catalysts are Al_2O_3 [38], SiO_2 [25], TiO_2 [39], Nb_2O_5 [40], and zeolites such as CHA and ZSM-5 [41–43].

However, all of the NH_3 SCO studies found in the literature are dedicated to catalytic combustion of ammonia. No reports can be found about the catalytic combustion of hydrogen ammonia mixtures or anything reassembling an ammonia SOFC off-gas. Thus, the results might not apply to the SOFC off-gas combustion.

Here, we report investigations about the combustion of ammonia SOFC off-gas surrogate over different catalysts with focus on mitigating NOx formation. Microstructured reactors coated with different supported noble and transition metal catalysts were used for the off-gas combustion and their performance in terms of NOx formation was evaluated and compared at different temperatures.

2. Results

2.1. Catalyst Characterisation

The metal-loadings of the calcined catalysts are close to the values targeted during preparation, as it gets evident from the XRF data summarized in Table 1. Only the rhodium and ruthenium-based catalysts contain higher amounts of the noble metals than the desired loading of 5 wt.-% active metal, with 5.79 and 6.50 wt.-%, respectively.

Table 1. Characterization results (XRD and TEM) for the prepared catalysts.

Catalyst	Metal Loading (XRF)/wt.-%	Particle Size (TEM)/nm
Pt/Al_2O_3	5.28	2.35
Pd/Al_2O_3	4.90	4.30
Rh/Al_2O_3	5.79	1.02
Ru/Al_2O_3	6.50	50.3
Ir/Al_2O_3	4.80	3.72
Ni/Al_2O_3	5.01	>30 nm
Fe/Al_2O_3	4.87	>25 nm
Cu/Al_2O_3	10.35	not measured

The XRD pattern (see Figures S1 and S2 in the supporting information) reveals no differences in the lines observed for alumina, thus it is evident that the aluminium support was not altered by the impregnation with the corresponding metals. The metal phases display distinctive diffraction lines in the XRD patterns. The identification of the metal phases according to the XRD pattern reveal that other that platinum, which is in elemental state, all other metals are present as oxides (palladium oxide PdO, rhodium oxide Rh_2O_3, ruthenium oxide RuO_2, iridium oxide IrO_2, nickel oxide (bunsenite) NiO, iron oxide (hematite) Fe_2O_3 and copper oxide (tenorite) CuO.

The nitrogen sorption isotherms of the different catalysts and the pure support Al_2O_3, shown in Figure S5 in the supporting information, are of IUPAC type II typical for mesoporous materials. The metal deposition did not alter the isotherms and thus did not change the textural properties significantly. This is also evident in the BET surface areas (see Supporting Information Table S1) of 147 to 154 $m^2\ g^{-1}$, which are slightly lower than the surface area of the pure Al_2O_3 support of 156 $m^2 \cdot g^{-1}$. The small reduction in surface area is likely caused by the lower specific surface area of the added metals. The surface area of the copper sample is further reduced to 140 $m^2 \cdot g^{-1}$ due to higher metal content.

The transmission electron microscopy (TEM) micrographs are shown in Figure 1 (higher magnification micrographs can be found in Figure S3 in the supporting information). The TEM images of all samples display amorphous Al_2O_3 particles as well as rod shaped Al_2O_3 crystallites. The metal phases as well as support material were identified using selected area electron diffraction (SAED). The SAED pattern and TEM images with the interplanar distances are shown in Figure S4 in the supporting information. Pt and Rh particles were determined to be in metallic state while all other metals are present as oxides (PdO, RuO_2, IrO_2, NiO, Fe_2O_3 and CuO). These results are in good accordance to the XRD data. Only exemption is rhodium which was identified as Rh_2O_3 by XRD and metallic rhodium by TEM.

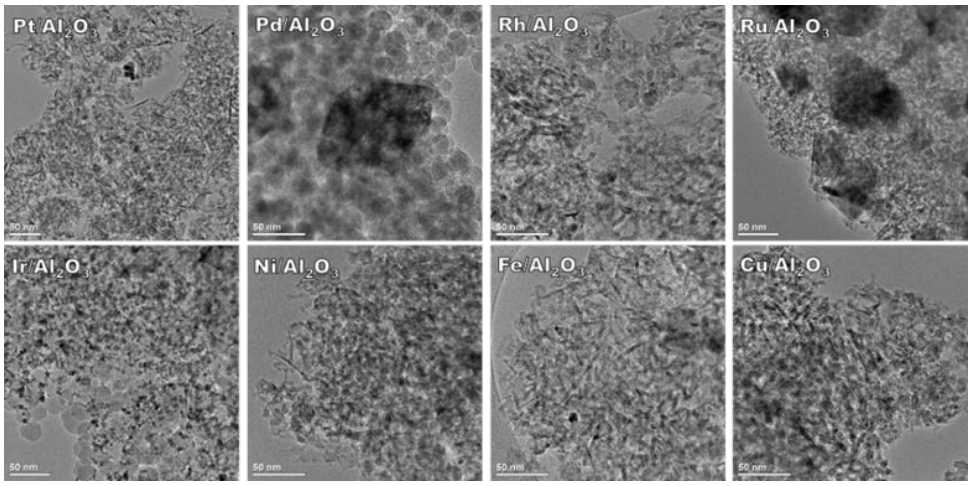

Figure 1. TEM micrographs of the different catalysts.

In case of Pt, Pd, Rh, Ru and Ir-based catalysts, the particles of the active metal phase are well dispersed over the support and can be seen easily due to their high molecular mass and thus high contrast. The average crystallite diameters can be found in Table 1. The CuO particles are hard to see and distinguish from the Al_2O_3 support, which made the measurement of a particle size distribution impractical. For the Ni and Fe-based catalysts, only a small numbers of large particles of the active phase could be seen on the TEM images.

2.2. Catalytic Tests

The evaluation of the catalytic activity was carried out under identical conditions applying a surrogate of ammonia SOFC off-gas with a composition as shown in Table 2. For the presented studies, the off-gas surrogate composition was chosen according to simulation results. For the simulation, the presumption was made that the off-gas will not be recycled in the SOFC, thus still contains a relative high concentration of hydrogen. Since the off-gas is not recycled, no separation of the water in the off-gas by condensation is necessary. Hence, the water content in the off-gas surrogate is very high. The model off-gas was mixed with air using an air-to-fuel ratio $\lambda = 4$ and then fed into the reactor.

Table 2. Composition of the model off-gas surrogate and feed gas used for the catalytic tests.

Component	SOFC Off-Gas Surrogate	Reactor Feed
N_2	25%	56.8%
H_2	15%	5.9%
NH_3	100 ppm	35.8 ppm
H_2O	60%	23.9%
O_2	-	13.2%

2.2.1. Noble Metal Catalysts

The noble metals platinum, palladium, rhodium, ruthenium and iridium supported on Al_2O_3 were tested as catalysts for the ammonia SOFC off-gas combustion. The hydrogen and ammonia concentrations as observed for different reaction temperatures are shown in Figure 2. Differences in low temperature activity of the catalysts tested are obvious.

For all tested noble metal-based catalysts, the hydrogen and ammonia conversions increase with increasing reaction temperature and reach complete conversion at about 400 °C latest. The lowest light off temperatures for hydrogen and ammonia are evident for the platinum catalyst, with full conversion of hydrogen at 150 °C and ammonia at 200 °C, respectively. The palladium-based catalyst shows a slightly reduced low temperature activity, reaching full conversion of hydrogen at 200 °C and ammonia 400 °C. The rhodium and iridium-based catalysts display comparable low temperature activity and reach full

conversion of hydrogen and ammonia at 400 °C. For the ruthenium-based catalyst, the lowest activity can be observed, with complete ammonia conversion at 400 °C and complete hydrogen conversion at 500 °C, respectively. Thus, the observed light off temperatures for hydrogen and ammonia increase in the order Pt < Pd < Rh < Ir < Ru.

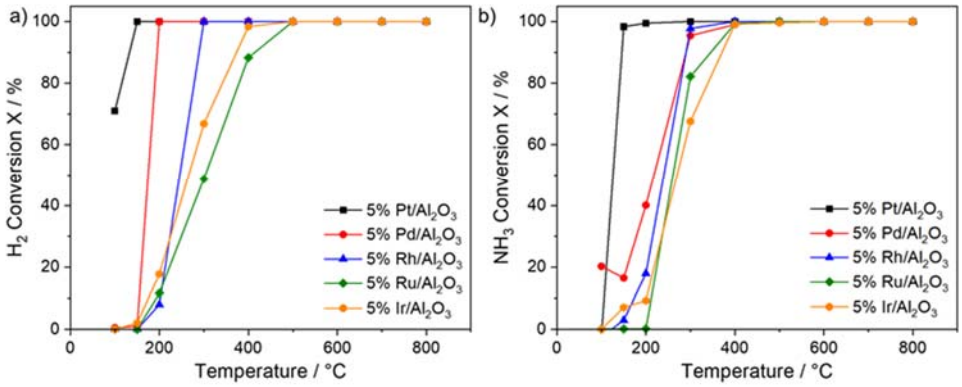

Figure 2. (**a**) Hydrogen and (**b**) ammonia conversion vs. reaction temperature for different noble metal catalysts, WHSV = 600 L/g h.

The concentrations of the nitrogen oxides (nitric oxide NO and nitrogen dioxide NO_2), shown in Figure 3a, reveal that ammonia is oxidized and forms nitrogen oxides (NO_x). Generally, once the reaction temperature is high enough for catalytic ammonia combustion, NO_x can be detected at the reactor outlet. Therefore, at low temperatures the tested catalysts show first NO_x formation according to their activity for ammonia combustion. With increasing reaction temperature, the observed NO_x concentrations increase and then stagnate at reaction temperatures exceeding 500 °C for all tested noble metal catalysts. At high temperatures in the range of 700 °C–800 °C, the NO_x concentrations increase in the order Ru < Rh < Ir < Pd < Pt.

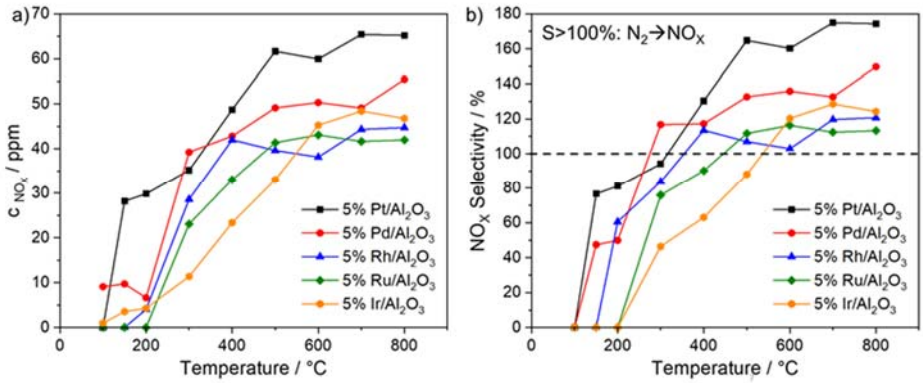

Figure 3. (**a**) NO_X concentration and (**b**) NO_X selectivities vs. reaction temperature for different noble metal catalysts, WHSV = 600 L/g h.

The different noble metal catalysts display differences in NO_X selectivity as summarized in Figure 3b. Interestingly, the measured NO_x concentrations at high temperatures exceed the ammonia concentration present in the off-gas feed of the reactor resulting in NO_x selectivities exceeding 100% if referred only to the NH_3 present in the feed. This indicates that the ammonia is completely converted into NO_x and a small fraction of the nitrogen is oxidized to NO_x as well, resulting in formation of additional NO_x. Especially the platinum catalyst displays a high additional NO_x formation, giving rise to a NO_x selectivity of about 170%. For the other noble metal catalysts high temperature NO_x selectivities between 115% and 140% were observed.

At lower temperatures, the observed NO_X molar flows are often lower than the converted ammonia resulting in NO_X selectivities lower than 100%. Therefore, it can

be assumed that at lower reaction temperatures a certain fraction of the ammonia is not converted into NO_x, but very likely into nitrogen. The selectivities to NO_x at 300 and 400 °C increase in order Ir<Ru<Rh<Pd<Pt. The lowest NO_x selectivity at full ammonia conversion of the tested noble metal catalysts was observed for the iridium catalyst with a NO_x selectivity of 63% at 400 °C.

The formation of nitrous oxide (N_2O) shows a different behaviour compared to the NO_x formation (see Figure 4). The N_2O concentrations have a maxima at 150 or 200 °C and with further increase in reaction temperature the N_2O concentration decreases. At 500 °C almost no N_2O is detectable at the reactor outlet for all tested noble metal catalysts.

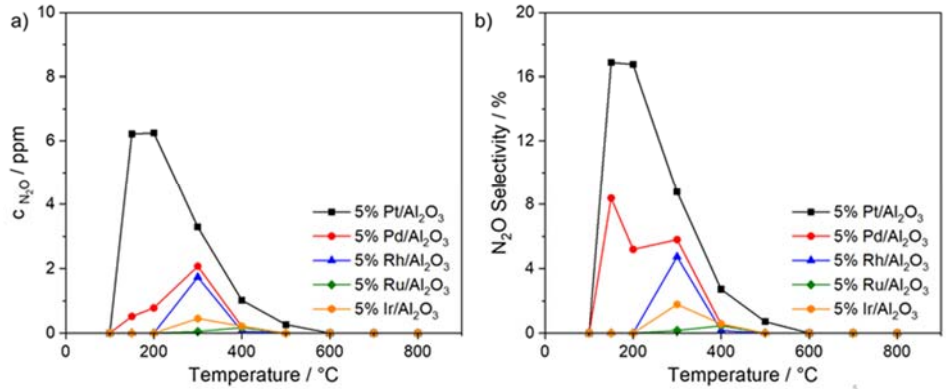

Figure 4. (**a**) N_2O concentration and (**b**) N_2O selectivities over reaction temperature for different noble metal catalysts, WHSV = 600 L/g h.

The highest N_2O concentrations are evident for the platinum catalyst, followed by palladium and rhodium. For the ruthenium and iridium catalysts almost no N_2O formation is observable, which can be traced back to the low activity of these catalysts at temperatures below 300 °C.

The selectivity to N_2O (see Figure 4b) follows the same trend as the N_2O concentrations, with exception of the palladium catalyst which shows an increased N_2O selectivity at 150 °C. The highest observed N_2O selectivity is 17% for the platinum catalyst. For all other noble metal catalyst N_2O selectivities below 10% can be observed.

Among the tested noble metals, iridium displays the most promising catalytic properties for the off-gas combustion. At a temperature of 400 °C, the iridium catalyst obtains complete hydrogen and ammonia conversion, low N_2O formation and comparatively low selectivity to NO_x.

2.2.2. Transition Metal Catalysts

In addition to noble metals, the transition metals iron, nickel and copper supported on alumina were tested as catalysts for the SOFC off-gas combustion and compared to the platinum catalyst. Both hydrogen and ammonia conversion follow the same trend as observed for the noble metal-based catalysts (see Figure 5). The differences in light off temperatures, however, are more pronounced for the transition metal catalysts. Again, with increasing reaction temperature both hydrogen and ammonia conversion increase for all tested transition metal-based catalysts. The nickel-based catalyst displays the highest activity of the tested transition metal catalyst, with complete hydrogen and ammonia conversion at 400 °C. The iron-based catalyst is slightly less active with full hydrogen and ammonia conversion at 400 °C and 600 °C, respectively. The copper-based catalyst shows a very low activity and thus high light off temperatures for both hydrogen and ammonia, despite its higher active metal loading of 10% compared to 5% for all other tested metals. To reach complete hydrogen and ammonia conversion over the copper-based catalyst a reaction temperature of about 600 °C is necessary.

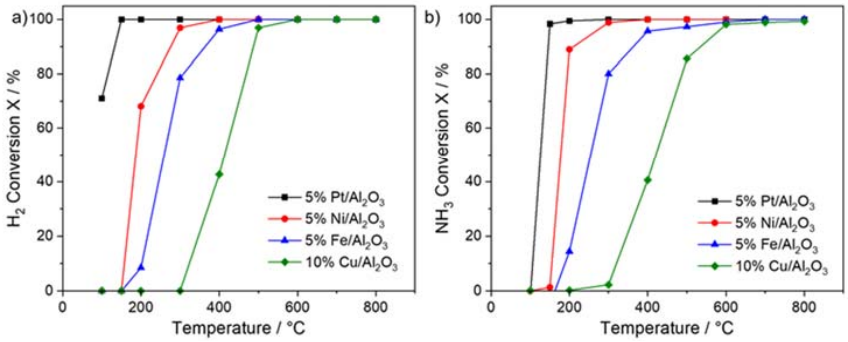

Figure 5. (**a**) Hydrogen and (**b**) ammonia conversion vs. reaction temperature for different transition metal catalysts, the platinum-based catalyst is shown for comparison, WHSV = 600 L/g h.

The NO_x concentrations observed for the tested transition metal catalysts are much lower compared to the platinum catalyst (see Figure 6a). The trend however is the same as for the noble metal catalysts. Once the reaction temperature is sufficiently high for catalytic ammonia combustion, NO_x can be detected at the reactor outlet. The NO_x concentrations and selectivities observed for the transition metal-based catalysts increase with reaction temperature and then stagnate at temperatures of 500 °C and above.

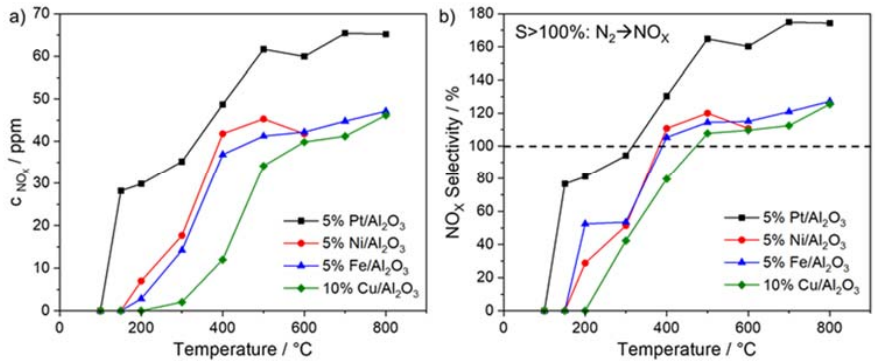

Figure 6. (**a**) NO_X concentration and (**b**) NO_X selectivity vs. reaction temperature for different transition metal catalysts, platinum-based catalyst shown for comparison, WHSV = 600 L/g h.

The nickel and iron-based catalysts display similar NO_x concentrations. However, since nickel is more active at low temperatures compared to iron, the nickel catalyst has a lower selectivity to NO_x below 500 °C as summarised in Figure 6b. The copper-based catalyst shows fairly low NO_x concentrations too, but the NO_x selectivity of the copper catalyst is higher than observed for iron and nickel. Again, at higher temperatures the NO_x concentrations surpass the ammonia concentration present in the feed gas and thus the NO_x selectivities are larger than 100%. This is a clear indication that at high temperatures NO_x is formed by ammonia combustion as well as by oxidation of nitrogen present in the off-gas.

Different studies have reported that copper oxides are good catalysts for ammonia combustion in terms of low NO_x selectivity. In our study the copper catalyst showed a much higher selectivity to NO_x compared to literature. However, the literature results were obtained for combustion in the absence of hydrogen. The presence of hydrogen could for example alter the oxidation state of copper in the catalyst which was proven to play an important role [26].

The formation of N_2O follows the same trend as observed for the noble metal catalysts (see Figure 7). At low temperatures the concentrations and selectivities increase with increasing ammonia conversions and reach a maximum at 200 °C to 300 °C. With further temperature increase the N_2O formation decreases and no N_2O can be overserved at temperatures exceeding 500 °C for all tested transition metal-based catalysts.

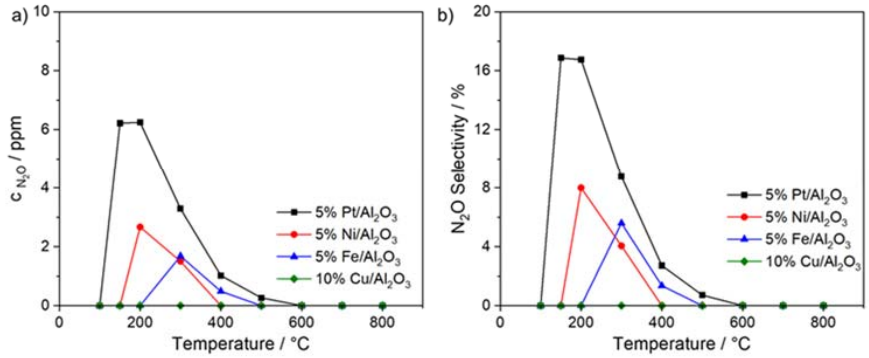

Figure 7. (**a**) N_2O concentration and (**b**) N_2O selectivity over reaction temperature for different transition metal catalysts, platinum-based catalyst shown for comparison, WHSV = 600 L/g h.

The nickel-based catalyst shows lower N_2O concentrations and selectivities compared to the platinum-based catalyst despite its relative high activity at 200 and 300 °C. At 400 °C no N_2O was observed for the nickel catalyst. The iron catalyst displays even lower N_2O concentrations but also lower activity at low temperatures resulting in slightly higher N_2O selectivity at 300 and 400 °C. No N_2O can be observed for the copper catalyst, likely because it is almost inactive at temperatures below 400°C, thus preventing N_2O formation as well.

Under the tested transitions of metal-based catalysts, the nickel-based catalyst displays the best performance. At a temperature of 300 °C, the nickel catalyst shows complete hydrogen and ammonia conversion with a rather low NO_x selectivity of 51%.

2.2.3. Catalyst Stability

Since the catalyst will be operated for prolonged times, catalytic stability was tested. A platinum catalyst was chosen for the experiments. The reaction was carried out at 800 °C with frequent cold starts from 100 to 800 °C.

The hydrogen conversion over time on stream in Figure 8a reveals that the catalyst fully converts the hydrogen even after prolonged reaction time at 800 °C. However, the hydrogen conversion during the cold start experiments (see Figure 8b) reveals catalyst deactivation. Initially during the first 24 h of reaction the catalyst loses activity as evident in the reduced hydrogen conversion at lower temperatures compared to the fresh catalyst.

With prolonged time on stream, no further reduction in hydrogen conversions can be observed. This indicated that the catalyst deactivation has stopped after the initial deactivation. Due to the observed catalyst deactivation the light-off temperature for hydrogen increases from below 100 °C to about 270 °C. Hence the preheating temperature necessary to start up the afterburner would be around 300 °C, which is still feasible.

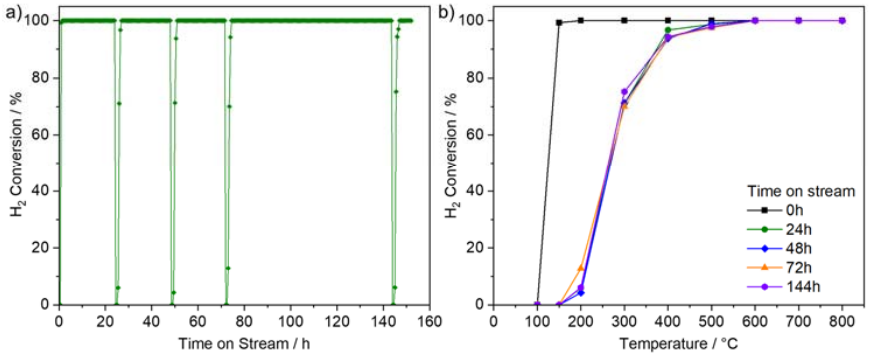

Figure 8. (**a**) Hydrogen conversion over time on stream with frequent cold start experiments and (**b**) hydrogen conversion over temperature for the corresponding cold start experiments after different times, catalyst 5% Pt/Al_2O_3, $T_{Reactor}$ = 800 °C (cold starts from 100 to 800 °C), WHSV = 600 L/g h.

3. Discussion

The light off temperatures for all tested catalysts, calculated at a 50% conversion level, for hydrogen and ammonia are summarized in Table 3. Despite the different homogenous light off temperatures for ammonia and hydrogen, the differences observed between hydrogen and ammonia light off are relatively small over all tested catalysts.

Table 3. Comparison of the catalytic performance of different metal-based catalysts tested in this study.

Catalyst	H_2 Light-Off $T_{X=50\%}$	NH_3 Light-Off $T_{X=50\%}$	Lowest S_{NOx} at X_{NH3}> 98%	S NOx at 600 °C
Pt/Al_2O_3	<100	125	81.1 (200 °C)	160.3
Pd/Al_2O_3	178	214	117.2 (400 °C)	135.9
Rh/Al_2O_3	243	244	113.6 (400 °C)	102.9
Ru/Al_2O_3	303	266	90.2 (400 °C)	116.4
Ir/Al_2O_3	267	275	63.1 (400 °C)	120.3
Ni/Al_2O_3	183	177	51.4 (300 °C)	110.7
Fe/Al_2O_3	257	254	115.0 (600 °C)	115.0
Cu/Al_2O_3	412	419	109.6 (600 °C)	109.6

Overall, platinum, nickel and palladium show low light-off temperatures, below 200 °C. For iridium, rhodium, iron and ruthenium the light–off temperatures are around 200 to 300 °C. For the copper-based catalyst the highest light-off temperature exceeding 400 °C can be observed, despite its higher loading of active metal on the catalyst support.

The selectivity to NO_x at 600 °C is close to the maximum, since the NO_x formation usually reaches a plateau at 600 °C. Here, the selectivity increases in the order Rh < Cu < Ni < Fe < Ru < Ir < Pd < Pt. The lowest selectivity to NO_x at full ammonia conversion (X_{NH3} > 98%) also corresponds to the lowest temperature necessary for full ammonia conversion since the NO_x selectivities increased with reaction temperature. The lowest value can be found for nickel and increases in the order Ni < Ir < Pt < Ru < Cu < Rh < Fe < Pd.

Comparison to Internal Combustion Engines

Compared to conventional internal combustion engines used for shipping, the presented NO_x emissions of the SOFC system are much lower.

NO_x emissions of maritime diesel engines are limited by regulation 13 of the MARPOL Annex VI of the International Maritime Organization (IMO). The current Tier II regulations set the NO_x limit at 14.4 g_{NOx}/kWh for slow running engines with rotational speeds of under 130 rpm and 7.7 g_{NOx}/kWh for engines running at over 2000 rpm.

The 2016 Tier III regulations by the IMO set more stringent NO_x limits in defined Emission Control Areas. In this areas, which include the Baltic and northern sea, the NO_x emission limits are 3.4 and 1.96 g_{NOx}/kWh, for engines operating at <130 and >2000 revolutions per minute, respectively. NO_x emission according to Tier II can be archived by modern diesel engines, Tier III however makes a deNO_x process such as ammonia-SCR necessary.

The presented system of NH_3 SOFC and afterburner emits 0.18 g NO_x per kWh (electric) in the worst case of complete NH_3 conversion to NO_2 at full load. Thus, the SOFC system only emits 9% of the NO_x emitted by Tier III conventional diesel engines. For the iridium and nickel-based catalysts developed in this work, values of about 5% of the specific NO_x emission of Tier III diesel engines can be obtained. The NO_x emission of the SOFC system were calculated at full load. Emissions are measured according to ISO 8178 at different loads which would lower the emissions even further.

Direct use of ammonia in internal combustion engines is possible too. Ammonia is partially split to hydrogen, since pure ammonia is not suitable for use in internal combustion engines. The ammonia/hydrogen mixture can be combusted at lower temperatures compared to diesel engines (CO_2 formation) and thus NO_x formation can be reduced.

Studies have shown that engines fuelled by hydrogen ammonia mixtures can achieve NO_x concentrations as low as 1−2 g NO_x per kWh depending of the ammonia concentration in the feed gas, which is still at least 10 times higher than the NO_x emissions of the NH_3 SOFC system.

Additionally, the tested catalysts were able to obtain complete conversion of ammonia at feasible operation temperatures for the afterburner, thus preventing ammonia slip from the SOFC system which can be a problem for ammonia-fuelled internal combustion engines.

4. Materials and Methods

4.1. Catalyst Preparation and Reactor Assembly

The investigations were carried out using microreactors containing microchannels coated with catalyst.

The reactors consisted of two plates with 14 channels each. The channels are 500 µm in width, 250 µm deep and 25 mm long. Once the two plates were welded together, channels with a depth of 500 µm were obtained.

The preparation and assembly consisted of three main steps: preparation of the catalyst powder, wash coating of the catalyst in the microchannels and finally assembly of the reactor via laser welding.

Catalyst powder preparation: The catalyst powders were prepared by impregnation of the Al_2O_3 support (Puralox, Sasol) with the calculated amount of an aqueous solution containing the corresponding metal precursor to archive the desired catalyst composition. After impregnation the samples were calcined at 450 °C for 6 h and the powders were milled and used for the wash coating. The metal precursors used were: $Pt(NH_3)_4(NO_3)_2$ (Alfa Aesar), $Ni(NO_3)_2{\cdot}6H_2O$ (Sigma-Aldrich), $Rh(NO_3)_3$ solution (chemPUR), $IrCl_3{\cdot}xH_2O$ (Alfa Aesar), $Fe(NO_3)_3{\cdot}9H_2O$ (Sigma-Aldrich), $Cu(NO_3)_2{\cdot}3H_2O$ (Honeywell / Fluka), $Pd(NO_3)_2$ solution (Sigma-Aldrich), $Ru(NO)(NO_3)_3$ (Alfa Aesar).

Wash coating: The microchannels were coated by using a suspension containing the catalyst powder, polyvinyl alcohol as binder, acetic acid and deionised water. The polyvinyl alcohol was dissolved in water at 65 °C for 3 h before 1 wt.-% acetic acid and the catalyst powder were added. The suspension was then stirred at 65 °C for additional 3 h followed by stirring at room temperature for 2–3 days to obtain a homogeneous suspension.

The microchannels were filled with the suspension and excess suspension was removed using a blade. Then the plates were dried at room temperature and calcined at 450 °C. The wash coating process was described in greater detail in previous publications [44].

Reactor assembly: The coated plates as well as the inlet and outlet capillaries were assembled via laser welding to form the microreactor. More details can be found in a previous publication [45,46].

4.2. Catalytic Testing

The catalyst coated microstructured reactors were placed in a steal heating block equipped with two heating cartridges and thermocouples and connected to the test rig.

The gas mixture consisting of nitrogen, hydrogen and 250 ppm ammonia was mixed with air and steam before it was fed into the reactor. The gases were dosed via Bronkhorst mass flow controllers. Steam was delivered by dosing liquid water using a Bronkhorst Cori-flow into an evaporator. All lines were heated to 180 °C to avoid condensation.

Ammonia concentrations were measured using a MKS FTIR spectrometer. The hydrogen concentration was measured using an Agilent µGC.

To obtain a weight hourly space velocity (WHSV) of 600 L/g h a catalyst mass of 20 to 25 mg was used and the flow rate adjusted accordingly. For example, for a catalyst mass of 20 mg the flow rates were set to 120.1 mL/min air, 31.98 mL/min off-gas surrogate and 2.31 g/h water, resulting in a total flow rate of 200 mL/min.

4.3. Catalyst Characterization

X-ray diffraction (XRD): X-ray diffraction measurements were carried out using a D8-Advance diffractometer (Bruker) equipped with Cu-K_α radiation source and LYNXEYE XT-E detector in Bragg-Brentano geometry from 5–90° 2Theta with a step size of 0.02°.

X-ray fluorescence (XRF): The elemental composition of the samples was measured by XRF spectroscopy on an ED-XRF spectrometer model 1510 (Canberra Packard, USA). As radiation source Cd-109 (22 keV) and Am-241 (60 keV) were used.

Transmission electron microscopy (TEM): the transmission electron microscopy images were taken on a Zeiss Libra 120 instrument operating at an accelerating voltage of 120 kV. Before the measurements, the catalyst samples were suspended in ethanol, dropped onto the TEM grids and dried.

Nitrogen physisorption: nitrogen sorption experiments were carried out at −273 °C using an Anton Parr Autosorb iQ. The samples were degassed for 12 h at 250 °C under vacuum before measurement.

5. Conclusions

The present study shows that it is possible to use an afterburner catalyst to completely combust both hydrogen and ammonia present in an ammonia SOFC off-gas stream. However, all tested catalysts oxidized at least parts of the ammonia to nitrogen oxides. The selectivity to NO_x increases with reaction temperature and reaches a plateau at about 600 °C. The formation of N_2O increases initially with increasing reaction temperature and reaches a maximum at about 200 to 300 °C. With further temperature increases, the N_2O formation decreases and no N_2O is detectable at temperatures between 400 and 500 °C, depending on the catalyst.

Compared to other studies reported in the literature, much higher NO_x selectivities were observed for the catalysts tested in this study. However, the studies in literature were dedicated to ammonia combustion without any other fuel present in the feed gas. The relative high concentration of hydrogen in the SOFC off-gas clearly alters the nitrogen selectivities of the catalysts.

Another difference is the WHSV used for the catalytic tests. The afterburner for the Ship-FC project needs to be cost effective and relatively small and light for use onboard a shipping vessel. Thus, the used WHSV of 600 L/g_{cat} h is high compared to the WHSV reported in literature.

Nevertheless, by selecting a suitable catalyst it is feasible to reduce the NO_X formation drastically, especially at low temperatures. Nevertheless, a complete mitigation of NO_X formation was not found possible using the presented catalyst systems.

Very promising candidates are nickel and iridium-based catalysts. The nickel-based catalyst shows the lowest NO_x selectivity in the low temperature range, as well as good cold start performance. However, operating the afterburner at low temperatures results in the formation of small quantities of N_2O. The observed N_2O concentration at 300 °C is below 2 ppm, and could be reduced by further catalyst optimization. For complete N_2O mitigation, iridium is the most promising active metal tested in this study.

The iridium-based catalyst has the smallest NO_x selectivities at 400 and 500 °C of all catalysts tested in this work. The selectivity to NO_x at 400 °C is higher compared to the nickel-based catalyst at 300 °C, but due to higher reaction temperature, the N_2O formation is suppressed completely. One drawback is the reduced cold start performance of iridium, with higher light off temperatures for both hydrogen and ammonia, compared to nickel, palladium and platinum-based catalysts.

In future, further reduction in NO_x emissions could be achieved by reducing the ammonia concentration in the off-gas, by further advancements in catalyst development or by removal of the formed NO_x. Studies to determine the effect of different catalyst supports, other active metals and bi-metallic catalysts could be beneficial to further reduce the NO_x formation in the afterburner. For the off-gas cleaning, well-established processes

such as catalytic selective reduction (SCR) of NO_x to N_2 with ammonia are available and could be implemented to lower NO_x emissions further.

Supplementary Materials: The following supporting information can be downloaded at: https://www.mdpi.com/article/10.3390/catal12101186/s1, Figure S1: Powder XRD pattern of noble metal-based catalysts; Figure S2: Powder XRD pattern of transition metal-based catalysts; Figure S3: TEM micrographs of the used catalysts with two different magnifications; Figure S4: TEM micrographs with interplanar distances and selected area electron beam diffraction images used for identification, Figure S5: Nitrogen sorption isotherm of Al_2O_3 support; Figure S6: Nitrogen sorption isotherms of the used catalysts, Figure S7: Particle size distribution of different catalysts determined by TEM, Table S1: Specific surface area (BET method) of the used catalysts.

Author Contributions: Conceptualization, G.K., H.P. and T.W.; investigation, T.W and R.Z.; writing—original draft preparation, T.W.; writing—review and editing, T.W., R.Z., H.P. and G.K.; visualization, T.W.; supervision, G.K.; project administration, H.P. and G.K.; funding acquisition, G.K. All authors have read and agreed to the published version of the manuscript.

Funding: This research was funded by the ShipFC project which has received funding from the Fuel Cells and Hydrogen Joint Undertaking under grant agreement No 875156. This Joint Undertaking receives support from the European Union's Horizon 2020 research and innovation program and from Hydrogen Europe.

Data Availability Statement: Not applicable.

Conflicts of Interest: The authors declare no conflict of interest.

References

1. Miola, A.; Ciuffo, B. Estimating air emissions from ships: Meta-analysis of modelling approaches and available data sources. *Atmos. Environ.* **2011**, *45*, 2242–2251. [CrossRef]
2. Balcombe, P.; Brierley, J.; Lewis, C.; Skatvedt, L.; Speirs, J.; Hawkes, A.; Staffell, I. How to decarbonise international shipping: Options for fuels, technologies and policies. *Energy Convers. Manag.* **2019**, *182*, 72–88. [CrossRef]
3. CAIT. *World Resources Institute. Historical Emissions Data*; World Resources Institute: Washington, DC, USA, 2017.
4. International Maritime Organization. *Initial IMO Strategy on Reduction of GHG Emissions from Ships*; International Maritime Organization: London, UK, 2018.
5. Stambouli, A.B.; Traversa, E. Fuel cells, an alternative to standard sources of energy. *Renew. Sustain. Energy Rev.* **2002**, *6*, 295–304. [CrossRef]
6. Xu, Q.; Kobayashi, T. *Advanced Materials for Clean Energy*; CRC Press: Boca Raton, FL, USA, 2019; ISBN 1482205807.
7. He, T.; Pachfule, P.; Wu, H.; Xu, Q.; Chen, P. Hydrogen carriers. *Nat. Rev. Mater.* **2016**, *1*, 16059. [CrossRef]
8. Wojcik, A.; Middleton, H.; Damopoulos, I. Ammonia as a fuel in solid oxide fuel cells. *J. Power Sources* **2003**, *118*, 342–348. [CrossRef]
9. Lan, R.; Irvine, J.T.S.; Tao, S. Ammonia and related chemicals as potential indirect hydrogen storage materials. *Int. J. Hydrogen Energy* **2012**, *37*, 1482–1494. [CrossRef]
10. Valera-Medina, A.; Xiao, H.; Owen-Jones, M.; David, W.I.F.; Bowen, P.J. Ammonia for power. *Prog. Energy Combust. Sci.* **2018**, *69*, 63–102. [CrossRef]
11. Minutillo, M.; Perna, A.; Di Trolio, P.; Di Micco, S.; Jannelli, E. Techno-economics of novel refueling stations based on ammonia-to-hydrogen route and SOFC technology. *Int. J. Hydrogen Energy* **2021**, *46*, 10059–10071. [CrossRef]
12. Afif, A.; Radenahmad, N.; Cheok, Q.; Shams, S.; Kim, J.H.; Azad, A.K. Ammonia-fed fuel cells: A comprehensive review. *Renew. Sustain. Energy Rev.* **2016**, *60*, 822–835. [CrossRef]
13. Jeerh, G.; Zhang, M.; Tao, S. Recent progress in ammonia fuel cells and their potential applications. *J. Mater. Chem. A* **2021**, *9*, 727–752. [CrossRef]
14. Siddiqui, O.; Dincer, I. A review and comparative assessment of direct ammonia fuel cells. *Therm. Sci. Eng. Prog.* **2018**, *5*, 568–578. [CrossRef]
15. Jiao, F.; Xu, B. Electrochemical ammonia synthesis and ammonia fuel cells. *Adv. Mater.* **2019**, *31*, 1805173. [CrossRef] [PubMed]
16. Chmielarz, L.; Jabłońska, M. Advances in selective catalytic oxidation of ammonia to dinitrogen: A review. *RSC Adv.* **2015**, *5*, 43408–43431. [CrossRef]
17. Sobczyk, D.P.; van Grondelle, J.; Thüne, P.C.; Kieft, I.E.; de Jong, A.; van Santen, R.A. Low-temperature ammonia oxidation on platinum sponge studied with positron emission profiling. *J. Catal.* **2004**, *225*, 466–478. [CrossRef]
18. Jabłońska, M.; Król, A.; Kukulska-Zajac, E.; Tarach, K.; Chmielarz, L.; Góra-Marek, K. Zeolite Y modified with palladium as effective catalyst for selective catalytic oxidation of ammonia to nitrogen. *J. Catal.* **2014**, *316*, 36–46. [CrossRef]

19. Chen, W.; Qu, Z.; Huang, W.; Hu, X.; Yan, N. Novel effect of SO_2 on selective catalytic oxidation of slip ammonia from coal-fired flue gas over IrO_2 modified Ce–Zr solid solution and the mechanism investigation. *Fuel* **2016**, *166*, 179–187. [CrossRef]
20. Shin, J.H.; Kim, G.J.; Hong, S.C. Reaction properties of ruthenium over Ru/TiO_2 for selective catalytic oxidation of ammonia to nitrogen. *Appl. Surf. Sci.* **2020**, *506*, 144906. [CrossRef]
21. Long, R.Q.; Yang, R.T. Noble metal (Pt, Rh, Pd) promoted Fe-ZSM-5 for selective catalytic oxidation of ammonia to N_2 at low temperatures. *Catal. Lett.* **2002**, *78*, 353–357. [CrossRef]
22. Zhang, L.; He, H. Mechanism of selective catalytic oxidation of ammonia to nitrogen over Ag/Al_2O_3. *J. Catal.* **2009**, *268*, 18–25. [CrossRef]
23. Lin, M.; An, B.; Niimi, N.; Jikihara, Y.; Nakayama, T.; Honma, T.; Takei, T.; Shishido, T.; Ishida, T.; Haruta, M. Role of the acid site for selective catalytic oxidation of NH_3 over Au/Nb_2O_5. *ACS Catal.* **2019**, *9*, 1753–1756. [CrossRef]
24. Long, R.Q.; Yang, R.T. Selective catalytic oxidation of ammonia to nitrogen over Fe_2O_3–TiO_2 prepared with a sol–gel method. *J. Catal.* **2002**, *207*, 158–165. [CrossRef]
25. Hinokuma, S.; Kiritoshi, S.; Kawabata, Y.; Araki, K.; Matsuki, S.; Sato, T.; Machida, M. Catalytic ammonia combustion properties and operando characterization of copper oxides supported on aluminum silicates and silicon oxides. *J. Catal.* **2018**, *361*, 267–277. [CrossRef]
26. Hirabayashi, S.; Ichihashi, M. Gas-phase reactions of copper oxide cluster cations with ammonia: Selective catalytic oxidation to nitrogen and water molecules. *J. Phys. Chem. A* **2018**, *122*, 4801–4807. [CrossRef] [PubMed]
27. Hinokuma, S.; Araki, K.; Iwasa, T.; Kiritoshi, S.; Kawabata, Y.; Taketsugu, T.; Machida, M. Ammonia-rich combustion and ammonia combustive decomposition properties of various supported catalysts. *Catal. Commun.* **2019**, *123*, 64–68. [CrossRef]
28. Amblard, M.; Burch, R.; Southward, B.W.L. A study of the mechanism of selective conversion of ammonia to nitrogen on Ni/γ-Al_2O_3 under strongly oxidising conditions. *Catal. Today* **2000**, *59*, 365–371. [CrossRef]
29. Lee, J.Y.; Kim, S.B.; Hong, S.C. Characterization and reactivity of natural manganese ore catalysts in the selective catalytic oxidation of ammonia to nitrogen. *Chemosphere* **2003**, *50*, 1115–1122. [CrossRef]
30. De Boer, M.; Huisman, H.M.; Mos, R.J.M.; Leliveld, R.G.; van Dillen, A.J.; Geus, J.W. Selective oxidation of ammonia to nitrogen over SiO_2-supported MoO_3 catalysts. *Catal. Today* **1993**, *17*, 189–200. [CrossRef]
31. Lee, S.M.; Hong, S.C. Promotional effect of vanadium on the selective catalytic oxidation of NH3 to N2 over Ce/V/TiO2 catalyst. *Appl. Catal. B Environ.* **2015**, *163*, 30–39. [CrossRef]
32. Song, S.; Jiang, S. Selective catalytic oxidation of ammonia to nitrogen over CuO/CNTs: The promoting effect of the defects of CNTs on the catalytic activity and selectivity. *Appl. Catal. B Environ.* **2012**, *117*, 346–350. [CrossRef]
33. Hung, C.-M.; Lai, W.-L.; Lin, J.-L. Removal of gaseous ammonia in Pt-Rh binary catalytic oxidation. *Aerosol Air Qual. Res.* **2012**, *12*, 583–591. [CrossRef]
34. Zhou, M.; Wang, Z.; Sun, Q.; Wang, J.; Zhang, C.; Chen, D.; Li, X. High-performance Ag–Cu nanoalloy catalyst for the selective catalytic oxidation of ammonia. *ACS Appl. Mater. Interfaces* **2019**, *11*, 46875–46885. [CrossRef] [PubMed]
35. Chmielarz, L.; Jabłońska, M.; Strumiński, A.; Piwowarska, Z.; Węgrzyn, A.; Witkowski, S.; Michalik, M. Selective catalytic oxidation of ammonia to nitrogen over Mg-Al, Cu-Mg-Al and Fe-Mg-Al mixed metal oxides doped with noble metals. *Appl. Catal. B Environ.* **2013**, *130*, 152–162. [CrossRef]
36. Chmielarz, L.; Kuśtrowski, P.; Rafalska-Łasocha, A.; Dziembaj, R. Selective oxidation of ammonia to nitrogen on transition metal containing mixed metal oxides. *Appl. Catal. B Environ.* **2005**, *58*, 235–244. [CrossRef]
37. Qu, Z.; Wang, Z.; Zhang, X.; Wang, H. Role of different coordinated Cu and reactive oxygen species on the highly active Cu–Ce–Zr mixed oxides in NH_3-SCO: A combined in situ EPR and O_2-TPD approach. *Catal. Sci. Technol.* **2016**, *6*, 4491–4502. [CrossRef]
38. Sun, M.; Liu, J.; Song, C.; Ogata, Y.; Rao, H.; Zhao, X.; Xu, H.; Chen, Y. Different reaction mechanisms of ammonia oxidation reaction on Pt/Al_2O_3 and $Pt/CeZrO_2$ with various Pt states. *ACS Appl. Mater. Interfaces* **2019**, *11*, 23102–23111. [CrossRef]
39. Jabłońska, M. TPR study and catalytic performance of noble metals modified Al_2O_3, TiO_2 and ZrO_2 for low-temperature NH_3-SCO. *Catal. Commun.* **2015**, *70*, 66–71. [CrossRef]
40. Lin, M.; An, B.; Takei, T.; Shishido, T.; Ishida, T.; Haruta, M.; Murayama, T. Features of Nb_2O_5 as a metal oxide support of Pt and Pd catalysts for selective catalytic oxidation of NH_3 with high N_2 selectivity. *J. Catal.* **2020**, *389*, 366–374. [CrossRef]
41. Akah, A.; Cundy, C.; Garforth, A. The selective catalytic oxidation of NH3 over Fe-ZSM-5. *Appl. Catal. B Environ.* **2005**, *59*, 221–226. [CrossRef]
42. Guo, J.; Yang, W.; Zhang, Y.; Gan, L.; Fan, C.; Chen, J.; Peng, Y.; Li, J. A multiple-active-site Cu/SSZ-13 for NH_3-SCO: Influence of Si/Al ratio on the catalytic performance. *Catal. Commun.* **2020**, *135*, 105751. [CrossRef]
43. Yue, Y.; Liu, B.; Qin, P.; Lv, N.; Wang, T.; Bi, X.; Zhu, H.; Yuan, P.; Bai, Z.; Cui, Q. One-pot synthesis of FeCu-SSZ-13 zeolite with superior performance in selective catalytic reduction of NO by NH_3 from natural aluminosilicates. *Chem. Eng. J.* **2020**, *398*, 125515. [CrossRef]
44. Zapf, R.; Thiele, R.; Wichert, M.; O'Connell, M.; Ziogas, A.; Kolb, G. Application of rhodium nanoparticles for steam reforming of propane in microchannels. *Catal. Commun.* **2013**, *41*, 140–145. [CrossRef]

45. Kolb, G.; Zapf, R.; Hessel, V.; Löwe, H. Propane steam reforming in micro-channels—results from catalyst screening and optimisation. *Appl. Catal. A Gen.* **2004**, *277*, 155–166. [CrossRef]
46. Zapf, R.; Becker-Willinger, C.; Berresheim, K.; Bolz, H.; Gnaser, H.; Hessel, V.; Kolb, G.; Löb, P.; Pannwitt, A.-K.; Ziogas, A. Detailed characterization of various porous alumina-based catalyst coatings within microchannels and their testing for methanol steam reforming. *Chem. Eng. Res. Des.* **2003**, *81*, 721–729. [CrossRef]